



Fermi National Accelerator Laboratory

FERMILAB-Conf-95/072-E

CDF

WW and WZ Production at the Tevatron

**Theresa A. Fuess
For the CDF Collaboration**

*Argonne National Laboratory
Argonne, Illinois 60439*

*Fermi National Accelerator Laboratory
P.O. Box 500, Batavia, Illinois 60510*

April 1995

**Published Proceedings *International Symposium on Vector Boson Self-Interactions*,
University of California at Los Angeles, Los Angeles, California, February 1-3, 1995**

Disclaimer

This report was prepared as an account of work sponsored by an agency of the United States Government. Neither the United States Government nor any agency thereof, nor any of their employees, makes any warranty, express or implied, or assumes any legal liability or responsibility for the accuracy, completeness, or usefulness of any information, apparatus, product, or process disclosed, or represents that its use would not infringe privately owned rights. Reference herein to any specific commercial product, process, or service by trade name, trademark, manufacturer, or otherwise, does not necessarily constitute or imply its endorsement, recommendation, or favoring by the United States Government or any agency thereof. The views and opinions of authors expressed herein do not necessarily state or reflect those of the United States Government or any agency thereof.

WW and WZ Production at the Tevatron

Theresa A. Fuess

Argonne National Laboratory
Argonne, Illinois 60439

Direct limits are set on WWZ and $WW\gamma$ three-boson couplings in a search for WW and WZ production in $p\bar{p}$ collisions at $\sqrt{s} = 1.8$ TeV using the DØ and CDF detectors at the Fermilab Tevatron.

INTRODUCTION

Among the most characteristic and fundamental signatures of non-Abelian symmetry of $SU(2) \times U(1)$ gauge theory of the Standard Model electroweak interactions are the interactions of W , Z , and γ bosons with each other. The interaction between the W and γ was previously studied in the process $p\bar{p} \rightarrow W\gamma$ (1). Here we report on bounds on the WWZ and $WW\gamma$ couplings obtained from the production of WW and WZ in $p\bar{p}$ interactions at $\sqrt{s} = 1.8$ TeV (2)

In the standard model, the dominant contribution to diboson production in $p\bar{p}$ collisions at $\sqrt{s} = 1.8$ TeV comes from two types of Feynman diagrams (figure 1). There are substantial cancellations between the t- or u-channel diagrams, which involve only the couplings of the bosons to fermions, and the s-channel diagrams which contain the three-boson coupling. These cancellations result in standard model cross sections of 9.5 pb and 2.5 pb for WW and WZ production respectively. To the extent that the fermionic couplings of the W , Z , and γ have been well tested, we may regard diboson production as primarily a test of the three-boson couplings.

The most general $WW\gamma$ and WWZ couplings consistent with Lorentz invariance have been formulated and may be parameterized in terms of fourteen

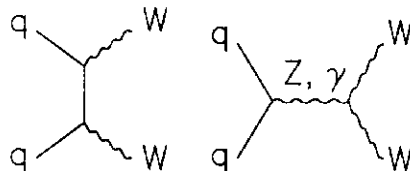


FIG. 1. Feynman diagrams for WW production. In the standard model there are substantial cancellations between these two types of diagrams.

independent couplings (or form factors), seven for the $WW\gamma$ vertex and seven for the WWZ vertex (3). They are $g_1^V, g_4^V, g_5^V, \lambda^V, \kappa^V, \tilde{\lambda}^V$, and $\tilde{\kappa}^V$ where V is either γ (for $WW\gamma$) or Z (for WWZ). The standard model $SU(2) \times U(1)$ electroweak theory corresponds to the choice $g_1^\gamma = g_1^Z = 1$ and $\kappa^\gamma = \kappa^Z = 1$ with all other couplings set to zero. The terms $\Delta\kappa \equiv \kappa - 1$ and $\Delta g_1 \equiv g_1 - 1$ are also used.

If any of these couplings differ substantially from the standard model values then the cross section increases. The enhancement is greatest at high boson P_T where the strongest cancellations occur in the standard model. Any couplings, differing from the standard model values, that are independent of $\sqrt{\hat{s}}$ cause the diboson production cross section to violate unitarity at some large $\sqrt{\hat{s}}$. To avoid this the anomalous parts of the couplings are made functions of $\sqrt{\hat{s}}$ and a form factor scale Λ_{FF} in such a way that they approach their standard model values when $\sqrt{\hat{s}}$ is bigger than Λ_{FF} .

$$\xi(\hat{s}) = \xi_{SM} + \frac{\xi(0) - \xi_{SM}}{(1 + \hat{s}/\Lambda_{FF}^2)^2} \quad (1)$$

where ξ stands for any of the couplings, ξ_{SM} is its value in the standard model, and Λ_{FF} represents the energy scale of unknown phenomena. The sensitivity of the measurement of the couplings can depend on the value of Λ_{FF} used. However, if Λ_{FF} is big enough, there is little effect at lower energies where the measurement is made.

The WW and WZ production at the Tevatron was studied in two channels, decay to leptons plus jets and decay to leptons only. The decay of WW, WZ to leptons plus jets gives better sensitivity to anomalous three-boson couplings than the purely leptonic channels because the leptonic branching fractions of the W and Z are small and because the acceptance of the detector for jets is larger than for leptons. Background from the QCD processes $p\bar{p} \rightarrow W + \text{jets}$ and $p\bar{p} \rightarrow Z + \text{jets}$ is greatly reduced by requiring a large boson P_T , while retaining good sensitivity to anomalous three-boson couplings (3). This measurement was made by CDF. The purely leptonic decay mode of WW does not have the overwhelming QCD W plus jets background and therefore allows observation of the predicted standard model signal with a direct measurement of the production cross section. This measurement was performed by both DØ and CDF. In both measurements the leptons include electrons and muons.

THE COLLIDER DETECTOR AT FERMILAB

The Collider Detector at Fermilab (CDF) has been described in detail elsewhere (4). Here we give a brief description of the components relevant to this analysis. The location of the event vertex is measured along the beam direction with a time projection chamber (VTX). The momenta of charged particles are measured in the central tracking chamber (CTC), which is surrounded by a 1.4 T superconducting solenoidal magnet. Outside the CTC, the calorimeter is organized in electromagnetic (EM) and hadronic (HAD) compartments with projective towers covering the pseudorapidity range $|\eta| \leq 3.6$.

Outside the central calorimeter, the region $|\eta| \leq 1.0$ is instrumented with drift chambers for muon identification.

Each electron is identified by an isolated cluster in either the central EM calorimeter ($|\eta| \leq 1.1$) which matches a track in the CTC or the endplug EM calorimeter ($1.1 \leq |\eta| \leq 2.4$) with associated hits in the VTX. Each muon is identified by an isolated track in the CTC with minimum ionizing energy in the calorimeter. Events with one or more muons must have at least one muon with matching hits in the muon chambers. The presence of neutrinos is inferred from missing transverse energy (\cancel{E}_T), which is measured by the magnitude of the vector sum of the calorimeter tower energies perpendicular to the beam axis. Jet energy is measured by clustering the EM and HAD calorimeter energy within a cone $\Delta R < 0.4$, where $\Delta R = \sqrt{\Delta\phi^2 + \Delta\eta^2}$, and ϕ is the azimuthal angle (5).

THE DØ DETECTOR

The DØ detector (6) consists of three major components: the calorimeter, tracking, and muon systems. A hermetic, compensating, uranium-liquid argon sampling calorimeter with fine transverse and longitudinal segmentation in projective towers measures energy out to $|\eta| \sim 4.0$, where η is the pseudorapidity. The energy resolution for electrons and photons is $15\%/\sqrt{E(\text{GeV})}$. The resolution for the transverse component of missing energy, $\cancel{E}_T^{\text{cal}}$, is $1.1 \text{ GeV} + 0.02(\sum E_T)$, where $\sum E_T$ is the scalar sum of transverse energy, E_T , in GeV, deposited in the calorimeter. The central and forward drift chambers are used to identify charged tracks for $|\eta| \leq 3.2$. There is no central magnetic field. Muons are identified and their momentum measured with three layers of proportional drift tubes, one inside and two outside of the magnetized iron toroids, providing coverage for $|\eta| \leq 3.3$. The muon momentum resolution, determined from $J/\psi \rightarrow \mu\mu$ and $Z \rightarrow \mu\mu$ events, is $\sigma(1/p) = 0.18(p-2)/p^2 \oplus 0.008$ (p in GeV/c). The p_T of identified muons is used to correct $\cancel{E}_T^{\text{cal}}$ to form the missing transverse energy, \cancel{E}_T .

Muons are required to be isolated, to have energy deposition in the calorimeter corresponding to at least that of a minimum ionizing particle, and to have $|\eta| \leq 1.7$. For the $\mu\mu$ channel, cosmic rays are rejected by requiring that the muons have timing consistent with the beam crossing. Electrons are identified through the longitudinal and transverse shape of isolated energy clusters in the calorimeter and by the detection of a matching track in the drift chambers. Electrons are required to be within a fiducial region of $|\eta| \leq 2.5$. A criterion on ionization (dE/dx), measured in the drift chambers, is imposed to reduce backgrounds from photon conversions and hadronic showers with large electromagnetic content.

CDF: $WW, WZ \rightarrow l\nu jj, lljj$

The data for this analysis were recorded with the Collider Detector at Fermilab during the 1992-93 Fermilab Tevatron collider run, corresponding to an integrated luminosity of 19.6 pb^{-1} . We search for WW and WZ event candidates consistent with the decay of one boson to leptons and the other to hadrons. Background QCD processes are calculated at Born level (7), including simulation of the CDF detector and jet fragmentation using an adaptation of the HERWIG program (8,9). The boson P_T requirement for WW and WZ event selection is chosen so that less than one background event is expected in the final sample. With this choice it is unnecessary to perform a background subtraction and any theoretical uncertainty in the background calculation is avoided.

A leptonic W decay is identified by an isolated electron or muon with $P_T > 20 \text{ GeV}/c$ and $\cancel{E}_T > 20 \text{ GeV}$ forming a transverse mass $M_T > 40 \text{ GeV}/c^2$. A leptonic Z decay is identified by an electron or muon pair of opposite charge forming an invariant mass $70 < M < 110 \text{ GeV}/c^2$. In events with a leptonic W or Z decay, a candidate hadronic W or Z decay is defined by the two jets (leading jets) in the event with the highest jet transverse energies (E_T). Each jet must have $E_T > 30 \text{ GeV}$ and the invariant mass of the jet pair must be in the range $60 < M_{JJ} < 110 \text{ GeV}/c^2$. The P_T of the two-jet system, interpreted as a hadronic W or Z decay, is required to satisfy $P_T > 130 \text{ GeV}/c$ for leptonic W events or $P_T > 100 \text{ GeV}/c$ for leptonic Z events.

The two-jet mass spectrum is shown in Figure 2a for events with a leptonic W decay and with both leading jets satisfying $E_T > 30 \text{ GeV}$. The sum of the predicted Standard Model WW and WZ signals plus QCD background is also shown, where the background is normalized to the observed number of W events with two jets minus the predicted signal. Figure 2b shows the two-jet P_T distribution in the subset of events which satisfy the two-jet mass criterion. The two-jet P_T requirement is indicated by the arrow. One event passes this cut. For events with a leptonic Z decay there are no events which satisfy all selection criteria.

The limits on the couplings follow from a Monte Carlo calculation of expected event yields for various values of the couplings. The Monte Carlo event generator (3,10) calculates to leading order the processes $p\bar{p} \rightarrow W^+W^-$ and $p\bar{p} \rightarrow WZ$ with subsequent decay of a W to $e\nu$, $\mu\nu$, or jj and a Z to $e\bar{e}$, $\mu\bar{\mu}$, or jj . Higher order QCD corrections to the cross section are accounted for by a "K-factor" of $K = 1 + \frac{8}{3}\pi\alpha_s$ (3). MTB2 structure functions are used (11). Initial and final state QCD radiation effects and jet fragmentation are modelled with an adaptation of HERWIG (8,9). The event generator is combined with a detector simulation which includes trigger efficiencies, lepton identification efficiencies, and jet response modeling. A fast parametrization of the full detector simulation was also employed. The trigger and lepton identification efficiencies are determined from the data and amount to 78% for electrons and 79% for muons. The modeling of the jet response and resolution are tuned to agree with studies of collider and test beam data (12).

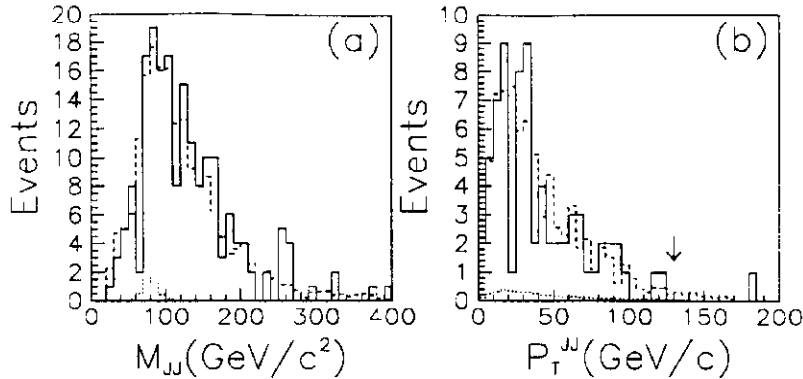


FIG. 2. CDF selection of $WW/WZ \rightarrow l\nu jj$ candidates. All event selection cuts except the two-jet mass and two-jet P_T cuts were used to select the events in (a). The subset of events from (a) passing the two-jet mass cut is shown in (b). One event remains after making all cuts. The solid line shows the data, the dots show the predicted standard model diboson signal, and the dashes show the predicted signal plus background shape.

The two-jet mass resolution is expected to be $9 \text{ GeV}/c^2$ for diboson events that would pass our candidate selection criteria. The efficiency of the two-jet mass cut is 88% for events passing all other cuts.

The systematic uncertainties on the yield are the uncertainties in the structure functions (6%), jet E_T scale and resolution (16%), luminosity (4%), lepton identification efficiency (1%), and trigger efficiency (1%). The Monte Carlo acceptance modeling has 3% statistical uncertainty, and a 5% systematic uncertainty allows for differences between fast and full detector simulations. In addition a 14% uncertainty is assigned for the effects of higher order QCD corrections (8,13,14). These uncertainties are combined in quadrature.

The acceptance is a strong function of the couplings, because of the boson P_T cut in combination with a varying boson P_T distribution. For standard model couplings, 0.13 $WW/WZ \rightarrow l\nu jj$ events and 0.02 $WZ \rightarrow lljj$ events are expected to pass the selection criteria, where l is either an electron or a muon. The observation of one event in the $l\nu jj$ channel and zero events in the $lljj$ channel is therefore not indicative of a departure from standard model couplings, even without consideration of the QCD background.

The predicted yield of high P_T boson pairs is a quadratic function of the anomalous couplings. The lack of an excess of events therefore results in bounds on the couplings which take the form of ellipses in the plane of any two couplings. Since the one event passing all selection criteria could be either signal or background, we calculate the confidence limits from the probability of observing one or less signal events. We do not perform a background subtraction and therefore obtain conservative limits. The probability distribution

used is the convolution of a Poisson distribution with a Gaussian, where the Gaussian smears the mean of the Poisson distribution around the expected yield within the systematic uncertainty.

In Figure 3 we present bounds on four pairs of couplings. Except as noted in the figure caption, for each case all the other couplings are fixed at the standard model values. Each pair is constrained to the interior of an ellipse, which is a two dimensional section through an ellipsoidal allowed region in the fourteen dimensional space of three boson couplings. Because the bosons are required to have high P_T our search is most sensitive to the couplings at energies near $\sqrt{s} = 500$ GeV. The limit contours, however, correspond to the value of the couplings at $\sqrt{s} = 0$ and therefore depend on the choice of Λ_{FF} according to equation (1). The bounds are shown for $\Lambda_{FF} = 1000$ GeV and $\Lambda_{FF} = 1500$ GeV. The unitarity bounds, which depend strongly on Λ_{FF} , are also shown (15,16). For values of Λ_{FF} larger than about 1600 GeV the bounds from unitarity are stronger than the bounds from the search.

Figure 3a shows limits in the plane λ^γ vs. λ^Z . The limits are stronger for λ^Z , illustrating the fact that the search is in general more sensitive to the WWZ couplings. It is therefore complementary to studies of the process $p\bar{p} \rightarrow W\gamma$ (1).

The limits of Figure 3b focus on the WWZ vertex, assuming that the $WW\gamma$ couplings take their standard model values. Bounds are shown for the couplings g_1^Z and κ^Z , which are the only WWZ couplings predicted to be nonzero in the standard model. The fact that the point $g_1^Z = \kappa^Z = 0$ lies outside the allowed region can be interpreted as direct evidence for a non-zero WWZ coupling, and for the resulting destructive interference between s-channel and t- or u-channel diagrams which takes place in the standard model. Specifically, the search is directly sensitive to the WWZ coupling in the region $\sqrt{s} = 500$ GeV. If the WWZ coupling were zero in this region, the s-channel diagram containing the WWZ vertex would not contribute to the amplitude, and the other diagrams by themselves would predict the observation of 15 ± 3 events, where the uncertainty is systematic. Independent of the choice of Λ_{FF} , this possibility is excluded at greater than 99% CL.

Figures 3c and 3d show limits on the couplings κ and λ , assuming specific relations between the WWZ and $WW\gamma$ couplings. In Figure 3c, the WWZ couplings are assumed to equal the $WW\gamma$ couplings. The resulting 95% CL limits on κ and λ separately, assuming that only one departs from its standard model value, are $-0.11 < \kappa < 2.27$ and $-0.81 < \lambda < 0.84$ for the choice $\Lambda_{FF} = 1000$ GeV. With the assumption of matching WWZ and $WW\gamma$ couplings, limits also result for the W boson electric quadrupole moment $Q_e^W = \frac{e}{M_W^2}(\kappa - \lambda)$ and magnetic dipole moment $\mu^W = \frac{e}{2M_W}(1 + \kappa + \lambda)$. In the standard model, these moments take the values $Q_e^W = \frac{e}{M_W^2}$ and $\mu^W = \frac{e}{M_W}$. The point $Q_e^W = \mu^W = 0$ is outside the allowed region. Assuming only one of the moments departs from its standard model value, the limits at 95% CL are $-2.42 < Q_e^W/(e/M_W^2) < 0.35$ and $0.37 < \mu^W/(e/M_W) < 1.70$ for $\Lambda_{FF} = 1000$ GeV.

For Figure 3d, the relation assumed between the WWZ and $WW\gamma$ cou-

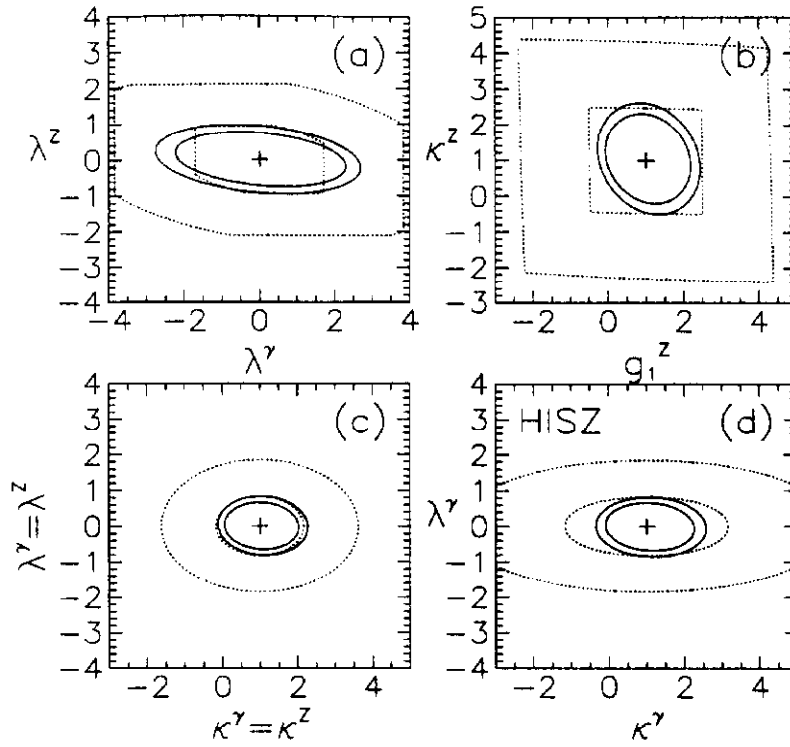


FIG. 3. CDF allowed regions for pairs of anomalous couplings from the analysis of $WW, WZ \rightarrow l\nu jj, lljj$ events. All couplings, other than those listed for each contour, are held at their standard model values. The solid lines are the 95% CL limits and the dotted lines are the unitarity limits; each is shown for $\Lambda_{\text{eff}} = 1000$ GeV (outer) and 1500 GeV (inner). The + signs indicate the Standard Model values of the couplings. (a) λ^γ and λ^z ; (b) g_1^z and κ^z ; (c) κ and λ assuming the WWZ and $WW\gamma$ couplings are the same; (d) $\kappa^\gamma, \kappa^z, \lambda^\gamma, \lambda^z$ and g_1^z in the HISZ prescription (see text), with independent variables κ^γ and λ^γ .

plings is given by the HISZ equations (17), which specify λ^Z , κ^Z , and g_1^Z in terms of the independent variables κ^γ and λ^γ . This prescription preserves $SU(2) \times U(1)$ gauge invariance and is well motivated in an effective Lagrangian approach. The corresponding subspace of anomalous couplings is not well constrained by previous indirect measurements (17). The individual 95% CL bounds on λ^γ and κ^γ are $-0.35 < \kappa^\gamma < 2.57$ and $-0.85 < \lambda^\gamma < 0.81$ for $\Lambda_{FF} = 1000$ GeV, if only one of the two is varied from its standard model value.

D0 : $WW \rightarrow l\nu l\nu$

The data for the D0 analysis were recorded during the 1992-93 collider run and correspond to an integrated luminosity of approximately 14 pb^{-1} . The D0 event samples come from triggers with dilepton signatures. The $e\mu$ sample is selected from events passing the trigger requirement of an electromagnetic cluster with $E_T \geq 7$ GeV and a muon with $p_T \geq 5$ GeV/c. The ee candidates are required to have two isolated electromagnetic clusters, each with $E_T \geq 10$ GeV. The $\mu\mu$ candidates are selected from events where at least one muon is identified with $p_T \geq 5$ GeV/c at the trigger level.

In the offline selection for the $e\mu$ channel, a muon with $p_T \geq 15$ GeV/c and an electron with $E_T \geq 20$ GeV are required. Both \cancel{E}_T and $\cancel{E}_T^{\text{cal}}$ are required to be ≥ 20 GeV. In order to suppress $Z \rightarrow \tau\bar{\tau}$ and $b\bar{b}$ backgrounds, it is required that $20^\circ \leq \Delta\phi(p_T^\mu, \cancel{E}_T) \leq 160^\circ$ if $\cancel{E}_T \leq 50$ GeV, where $\Delta\phi(p_T^\mu, \cancel{E}_T)$ is the angle in the transverse plane between the muon and \cancel{E}_T . One event survives these selection cuts in a data sample corresponding to an integrated luminosity of $13.5 \pm 1.6 \text{ pb}^{-1}$.

For the ee channel, two electrons are required, each with $E_T \geq 20$ GeV. The \cancel{E}_T is required to be ≥ 20 GeV. The Z boson background is reduced by removing events where the dielectron invariant mass is between 77 and 105 GeV/c². It is required that $20^\circ \leq \Delta\phi(p_T^e, \cancel{E}_T) \leq 160^\circ$ for the lower energy electron if $\cancel{E}_T \leq 50$ GeV. This selection suppresses $Z \rightarrow ee$ as well as $\tau\tau$. The integrated luminosity in this channel is $13.9 \pm 1.7 \text{ pb}^{-1}$. One event survives these selection requirements.

For the $\mu\mu$ channel, two muons are required, one with $p_T \geq 20$ GeV/c and another with $p_T \geq 15$ GeV/c. In order to remove Z boson events, it is required that the \cancel{E}_T projected on the dimuon bisector in the transverse plane be greater than 30 GeV. This selection requirement is less sensitive to the momentum resolution of the muons than is a dimuon invariant mass cut. It is required that $\Delta\phi(p_T^\mu, \cancel{E}_T) \leq 170^\circ$ for the higher p_T muon. No events survive these selection requirements in a data sample corresponding to an integrated luminosity of $11.8 \pm 1.4 \text{ pb}^{-1}$.

Finally, in order to suppress background from $t\bar{t}$ production, the vector sum of the E_T from hadrons, \vec{E}_T^{had} , defined as $-(\vec{E}_T^{h1} + \vec{E}_T^{h2} + \vec{E}_T^{\text{had}})$ is required to be less than 40 GeV in magnitude for all channels. Figure 4 shows a Monte Carlo simulation of \vec{E}_T^{had} for $\sim 20 \text{ fb}^{-1}$ of SM WW and $t\bar{t}$ events. For WW events, non-zero values of \vec{E}_T^{had} are due to gluon radiation and detector resolution.

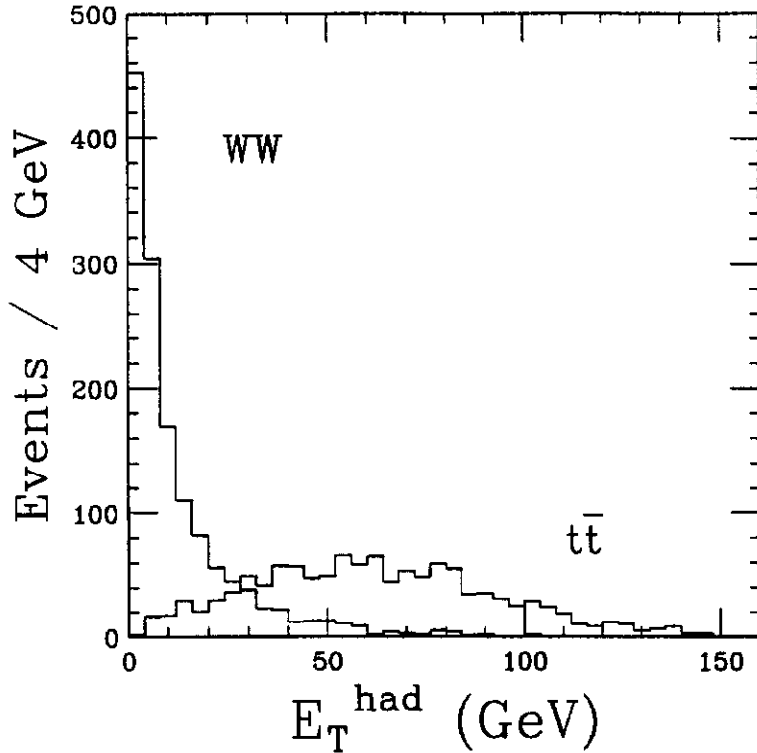


FIG. 4. E_T^{had} for Monte Carlo WW and $t\bar{t}$ events with $M_{t\text{op}} = 160 \text{ GeV}/c^2$ ($\int L dt \sim 20 \text{ fb}^{-1}$). Events with $E_T^{\text{had}} \geq 40 \text{ GeV}$ were rejected.

For $t\bar{t}$ events, the most significant contribution is the b -quark jets from the t -quark decays. This selection reduces the background from $t\bar{t}$ production by a factor of four for a t -quark mass of $160 \text{ GeV}/c^2$ and is slightly more effective for a more massive t -quark. The efficiency of this selection criterion for SM W boson pair production events is $0.95^{+0.01}_{-0.04}$ and decreases slightly with increasing W boson pair invariant mass. The surviving ee candidate passes this selection requirement but the $e\mu$ candidate (18) is rejected.

The detection efficiency for SM W boson pair production events is determined using the PYTHIA (19) event generator followed by a detailed GEANT (20) simulation of the DØ detector. Muon trigger and electron identification efficiencies are derived from the data. The overall detection efficiency for SM $WW \rightarrow e\mu$ is 0.092 ± 0.010 . For the ee channel the efficiency is 0.094 ± 0.008 . For the $\mu\mu$ channel it is 0.033 ± 0.003 . For the three channels combined, the expected number of events for SM W boson pair production, based on a cross section of 9.5 pb (13), is 0.46 ± 0.08 . The Monte Carlo program of Ref. (3)

Background	$e\mu$	ee	$\mu\mu$
$Z \rightarrow ee$ or $\mu\mu$	—	0.02 ± 0.01	0.066 ± 0.026
$Z \rightarrow \tau\tau$	0.11 ± 0.05	$< 10^{-3}$	$< 10^{-3}$
Drell-Yan dileptons	—	$< 10^{-3}$	$< 10^{-3}$
$W\gamma$	0.04 ± 0.03	0.02 ± 0.01	—
QCD	0.07 ± 0.07	0.15 ± 0.08	$< 10^{-3}$
$t\bar{t}$	0.04 ± 0.02	0.03 ± 0.01	0.009 ± 0.003
Total	0.26 ± 0.10	0.22 ± 0.08	0.075 ± 0.026

TABLE 1. DØ summary of backgrounds to $WW \rightarrow ee$, $WW \rightarrow e\mu$ and $WW \rightarrow \mu\mu$ events. The units are expected number of background events in the data sample. The uncertainties include both statistical and systematic contributions.

followed by a fast detector simulation (21) is used to estimate the detection efficiency for W boson pair production as a function of the coupling parameters λ and κ . The backgrounds due to Z boson, Drell-Yan dilepton, $W\gamma$, and $t\bar{t}$ events are estimated using the PYTHIA and ISAJET (22) Monte Carlo event generators followed by the GEANT detector simulation. The backgrounds from $b\bar{b}$, $c\bar{c}$, multi-jet, and W + jet events, where a jet is mis-identified as an electron, are estimated using the data. The $t\bar{t}$ cross section estimates are from calculations of Laenen *et al.* (23). The $t\bar{t}$ background is averaged for $M_{\text{top}} = 160, 170, \text{ and } 180 \text{ GeV}/c^2$. The background estimates are summarized in Table 1.

The 95% confidence level upper limit on the W boson pair production cross section is estimated based on one signal event including a subtraction of the expected background of 0.56 ± 0.13 events. The branching ratio $W \rightarrow l\bar{\nu} = 0.108 \pm 0.004$ (24) is assumed. Poisson-distributed numbers of events are convoluted with Gaussian uncertainties on the detection efficiencies, background and luminosity. For SM W boson pair production, the upper limit for the cross section is 91 pb at the 95% confidence level. From the observed limit, as a function of λ and κ , and the theoretical prediction of the W boson pair production cross section, the 95% confidence level limits on the coupling parameters shown in Figure 5 (solid line) are obtained. Also shown in Figure 5 (dotted line) is the contour of the unitarity constraint on the coupling limits for the form factor scale $\Lambda = 900 \text{ GeV}$. This value of Λ is chosen so that the observed coupling limits lie within this ellipse. The limits on the CP-conserving anomalous coupling parameters are $-2.6 < \Delta\kappa < 2.8$ ($\lambda = 0$) and $-2.2 < \lambda < 2.2$ ($\Delta\kappa = 0$).

CDF: $WW \rightarrow l\nu l\nu$

The data for the CDF analysis of WW in the purely leptonic mode (25) were taken during the 1992-93 and 1994 Tevatron collider runs and corresponds to an integrated luminosity of 45 pb^{-1} . The electron and muon selection are similar to that used in the CDF top search (26). Events were required to have

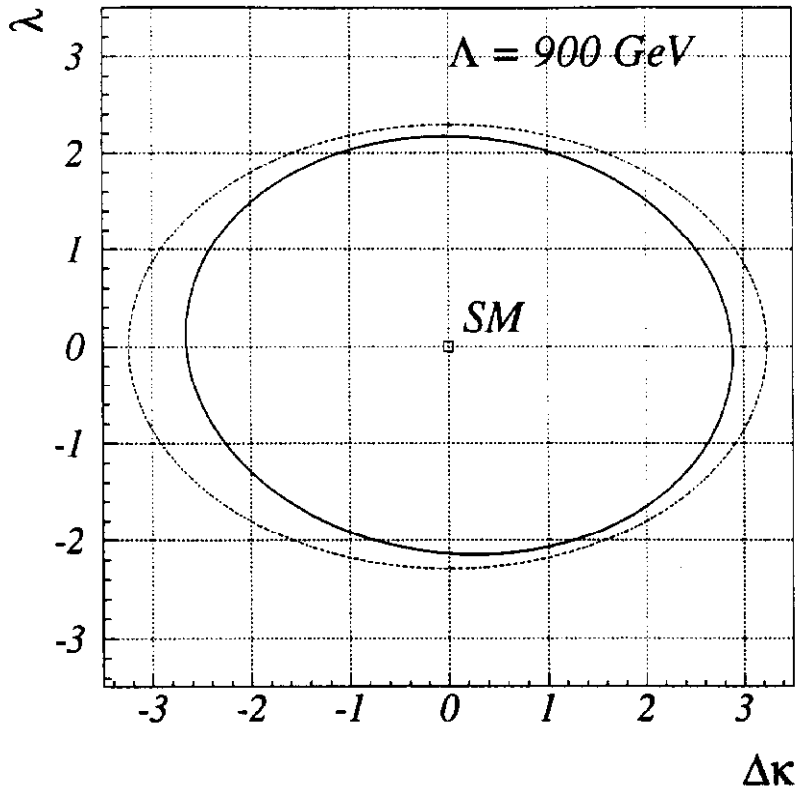


FIG. 5. DØ 95% CL limits on the CP-conserving anomalous couplings λ and $\Delta\kappa$, assuming that $\lambda_\gamma = \lambda_Z$ and $\kappa_\gamma = \kappa_Z$. The dotted contour is the unitarity limit for the form factor scale $\Lambda = 900 \text{ GeV}$ which was used to set the coupling limits.

Background in 19.3 pb^{-1}	$e\mu, ee, \mu\mu$
$Z \rightarrow ee, \mu\mu, \tau\tau$	0.03
$t\bar{t}$	0.06
$b\bar{b}$	0.07
Fake leptons	0.22
Total	0.38

TABLE 2. CDF summary of backgrounds to $WW \rightarrow ee, e\mu$, and $\mu\mu$ events. The units are expected number of background events in 19.3 pb^{-1} .

$E_T > 25 \text{ GeV}$ and $\Delta\Phi > 20 \text{ deg}$, where $\Delta\Phi$ is the angle between the E_T vector and the momentum of the charged lepton. Events are rejected if there is any jet with $E_T > 10 \text{ GeV}$ or if there are two oppositely charged leptons with an invariant mass in the Z mass window, $75\text{-}105 \text{ GeV}/c^2$. Two events pass all cuts compared to the Standard Model prediction of 1.3 WW events and 0.38 background events. The predicted background is outlined in Table 2

The resulting WW production cross section is found to be $7.9^{+11.4}_{-7.9} \pm 2.2 \text{ pb}$. The 95% confidence level upper limit on this cross section is 39.5 pb. The 95% confidence level limits on the couplings are $-1.8 < \Delta\kappa < 1.9$ ($\lambda = 0$) and $-1.4 < \Delta\lambda < 1.4$ ($\Delta\kappa = 0$) assuming $\Delta\kappa^Z = \Delta\kappa^\gamma$ and $\lambda^Z = \lambda^\gamma$ and that the acceptance is independent of $\Delta\kappa$ and λ .

CONCLUSIONS

In conclusion, a search for WW and WZ in $p\bar{p}$ collisions at $\sqrt{s} = 1.8 \text{ TeV}$ is made. The resulting limits on the trilinear couplings and on WW production are summarized in Table 3.

ACKNOWLEDGEMENTS

We thank U. Baur, T. Han and D. Zeppenfeld for Monte Carlo programs and for many stimulating discussions. We thank the Fermilab staff and the technical staffs of the participating institutions for their vital contributions. This work was supported by the U.S. Department of Energy and National Science Foundation; the Italian Istituto Nazionale di Fisica Nucleare; the Ministry of Education, Science and Culture of Japan; the Natural Sciences and Engineering Research Council of Canada; the National Science Council of the Republic of China; the A. P. Sloan Foundation; and the Alexander von Humboldt-Stiftung; the Commissariat a L'Energie Atomique in France; the Ministry for Atomic Energy and the Ministry of Science and Technology Policy in Russia; CNPq in Brazil; the Departments of Atomic Energy and Science and Education in India; Colciencias in Colombia; CONACyT in Mexico; and the Ministry of Education, Research Foundation and KOSEF in Korea.

Experiment process luminosity	Λ_{ff} (GEV)	assumptions	95% CL limits
<u>DØ</u> $WW \rightarrow l\nu l\nu$ 14 pb ⁻¹	900	$WWZ = WW\gamma$	$\Delta\kappa \in (-2.6, 2.8)$ $\lambda \in (-2.2, 2.2)$ $\sigma(p\bar{p} \rightarrow WW) < 91\text{pb}$
<u>CDF</u> $WW \rightarrow l\nu l\nu$ 45 pb ⁻¹	1000	$WWZ = WW\gamma$	$\Delta\kappa \in (-1.8, 1.9)$ $\lambda \in (-1.4, 1.4)$ $\sigma(p\bar{p} \rightarrow WW) < 40\text{pb}$
<u>CDF</u> $WW, WZ \rightarrow l\nu jj, lljj$ 19.6 pb ⁻¹	1000	$WWZ = WW\gamma$	$\Delta\kappa \in (-1.1, 1.3)$ $\lambda \in (-0.8, 0.8)$ $Q_s^W = \mu^W = 0$ is ruled out.
		$\kappa^\gamma = g_1^\gamma = 1$	$\kappa^Z = g_1^Z = 0$ is ruled out.
		HISZ	$\Delta\kappa^\gamma \in (-1.4, 1.5)$ $\lambda^\gamma \in (-0.8, 0.8)$ $\Delta\kappa^Z \in (-0.5, 0.5)$ $\lambda^Z \in (-0.8, 0.8)$ $\Delta g_1^Z \in (-0.9, 1.0)$

TABLE 3. Summary of limits set on $WW\gamma$ and WWZ trilinear couplings and on WW production at the Tevatron. All couplings, other than those for which limits are shown and those under HISZ, are held at their standard model values.

REFERENCES

1. J. Alitti *et al.*, *Phys. Lett. B* **277**, 194 (1992); F. Abe *et al.*, *Phys. Rev. Lett.* **74**, 1936 (1995); S. Abachi *et al.*, FERMILAB-PUB-95/0XX-E (1995), submitted to *Phys. Rev. Lett.*; H. Iahara, these proceedings.
2. F. Abe *et al.*, FERMILAB-PUB-95/036-E (1995), submitted to *Phys. Rev. Lett.* Mar 7, 1995; S. Abachi *et al.*, FERMILAB-PUB-95/044-E (1995), submitted to *Phys. Rev. Lett.* Mar 10, 1995.
3. K. Hagiwara *et al.*, *Phys. Rev. D* **41**, 2113 (1990).
4. F. Abe *et al.*, *Nucl. Instrum. Methods A* **271**, 387 (1988).
5. F. Abe *et al.*, *Phys. Rev. D* **45**, 1448 (1992).
6. S. Abachi *et al.*, *Nucl. Instrum. Methods A* **338**, 185 (1994).
7. F. A. Berends *et al.*, *Nucl. Phys. B* **357**, 32 (1991).
8. G. Marchesini *et al.*, *Comp. Phys. Comm.* **67**, 465 (1992).
9. J. Benlloch, *The Fermilab Meeting*, Proceedings of the Division of Particles and Fields of the APS, Batavia, IL, edited by C. H. Albright *et al.* (World Scientific, Singapore, 1993), p. 1091.
10. D. Zeppenfeld, private communication.
11. J. Morfin and W. K. Tung, *Z. Phys. C* **52**, 13 (1991).
12. F. Abe *et al.*, *Phys. Rev. Lett.* **68**, 1104 (1992).
13. J. Ohnemus, *Phys. Rev. D* **44**, 1403 (1991); J. Ohnemus, *Phys. Rev. D* **44**, 3477 (1991); U. Baur *et al.*, FSU-HEP-941010 (October 1994).
14. T. Han, private communication; V. Barger *et al.*, *Phys. Rev. D* **41**, 2782 (1990).
15. U. Baur and D. Zeppenfeld, *Phys. Lett. B* **201**, 383 (1988).
16. U. Baur, private communication.
17. K. Hagiwara *et al.*, *Phys. Rev. D* **48**, 2182 (1993); and references therein.
18. DØ Collaboration, S. Abachi *et al.*, *Phys. Rev. Lett.* **72**, 2138 (1994). The kinematic properties of this $t\bar{t}$ candidate are discussed in detail.
19. T. Sjöstrand, "PYTHIA 5.6 and Jetset 7.3 Physics and Manual," CERN-TH.6468/92, 1992, (unpublished).
20. F. Carminati *et al.*, "GEANT Users Guide," CERN Program Library, December 1991 (unpublished).
21. H. Johari, Ph. D. thesis, Northeastern University, 1995 (unpublished).
22. F. Paige and S. Protopopescu, BNL Report BNL38034, 1986 (unpublished), release V6.49.
23. E. Laenen, J. Smith, and W. L. van Neerven, *Phys. Lett. B* **321**, 254 (1994). For the $t\bar{t}$ background, the central value estimate of the cross section is used.
24. Particle Data Group, L. Montanet *et al.*, *Phys. Rev. D* **50**, 1173 (1994). The weighted average of the $W \rightarrow e\nu$ and $W \rightarrow \mu\nu$ branching fraction data is used.
25. See L. Zhang in these proceedings for more details.
26. F. Abe *et al.*, *Phys. Rev. D* **50**, 2966 (1994).